12th International Conference on Fracture Mechanics of Concrete and Concrete Structures
FraMCoS-12
B.L.A. Pichler, Ch. Hellmich, P. Preinstorfer (Eds)

https://doi.org/10.21012/FC12.1262
MS03-1:4

ADVANCED MICROSTRUCTURAL ANALYSIS OF CEMENT-BASED MATERIALS: INTEGRATING X-RAY COMPUTED TOMOGRAPHY AND DEEP LEARNING FOR ENHANCED CRACK GROWTH UNDERSTANDING

C. KUANG[*], N. BIN JAMAL M[†], A. MICHEL[#]

[*†#]Technical University of Denmark, Sustain

e-mail: ckuang@dtu.dk, nbjma@dtu.dk, almic@dtu.dk

Keywords: Fatigue damage, cement-based materials, deep learning

Abstract: Understanding the mechanism of crack growth in cement-based materials under mechanical loading involves complex interactions between microstructural components, including aggregates, voids, and cement paste. This paper presents a unique approach that combines X-ray computed tomography (XCT) with deep learning to segment these components precisely. By leveraging XCT's high-resolution 3D imaging capabilities and the robustness of deep learning algorithms, our method provides a detailed characterization of the microstructure of cement-based materials. This detailed structural information is crucial for understanding crack initiation and propagation processes, ultimately contributing to developing more durable and sustainable concrete. Our results highlight the significant potential of deep learning in enhancing our understanding of damage and failure mechanisms in cement-based materials, providing valuable insights that can lead to improved material performance and longevity.

1 INTRODUCTION

Cement-based materials are indispensable to civil infrastructure, yet their durability under cyclic loading remains a critical challenge, especially with increasing traffic demands and novel applications [1, 2]. Despite extensive research, the fatigue damage mechanisms in these heterogeneous materials are not fully understood, primarily due to the complex interactions among their microstructural components: the cement matrix, aggregates, and the interfacial transition zone (ITZ) [3, 4].

Two dominant hypotheses have emerged to explain fatigue damage: progressive deterioration of the ITZ[5], often considered the microstructure's weakest link and the initiation and propagation of microcracks within the cement matrix [6-9]. Understanding the relative contributions of these mechanisms is vital for developing fatigue-life prediction models. However, the microscopic scale of damage initiation under cyclic loading poses significant experimental challenges [4].

Experimental challenges in observing localized, phase-specific damage evolution have hindered progress in linking microstructural behavior to overall fatigue performance [2, 4]. Conventional cyclic loading experiment results, such as Stress/Strain-Number of cycles (S-N) curves, provide bulk insights but fail to capture the spatial and phase-specific processes driving fatigue. Scanning electron microscopy (SEM), on the other hand, requires destructive sample preparation that can introduce artifacts and alter the damage state, making it difficult to track damage progression accurately[10]. While methods reliance on indirect indicators like stress waves (AE)[11, 12], surface displacements (DIC)[13], or changes in wave velocity (UPV)[14], may not directly visualize the processes like crack initiation and propagation within the material, particularly

around the ITZ . To overcome these limitations, researchers have turned to non-destructive techniques like XCT, which allows for the visualization of internal damage features such as microcracks, providing a more comprehensive understanding of damage evolution [4, 15, 16]. However, its high-resolution data pose significant challenges for analysis, particularly in accurately differentiating and linking damage mechanisms to specific microstructural features within heterogeneous phases [4, 16].

This study integrates in-situ XCT imaging with an advanced semantic segmentation model based on a 2D U-Net architecture with a ResNet50 encoder and SCSE attention mechanisms to address these challenges. This innovative approach facilitates precise phase-specific segmentation, enabling a detailed examination of the complex interactions between ITZ degradation and matrix microcrack growth during fatigue. To capture detailed microstructural changes, the experimental setup involved cyclic loading of cylindrical mortar samples, scanned at critical loading intervals. This methodology provides a non-destructive framework for visualizing and analyzing the interplay between microstructural phases, offering new opportunities to study fatigue behavior in cementitious materials.

2 METHODOLOGY

2.1 In-situ XCT imaging under cyclic loading

Cylindrical mortar samples with a diameter of 7 mm and a height of 14.8 mm were prepared and analyzed, as described in our previous study[17]. The in-situ XCT setup included a micromechanical device (CT5000, Deben) and an X-ray microscope (Zeiss X-radia Versa 520) at DTU's 3D Imaging Center. Scanning parameters were set to 100 kV voltage, 8 W power, 0.4× magnification, and 3 seconds exposure time. Each scan, comprising 801 projections over 360°, lasted 1 hour and 21 minutes, with a voxel size of approximately $(13.88\ \mu m)^3$.

The sample underwent cyclic loading from 600 N (15.6 MPa) to 2000 N (52.0 MPa). Scans were taken at 600 N after 0, 10, 50, and 200 cycles, with the 0th cycle representing the initial scan after the sample was firstly monotonicly loaded to 600 N.

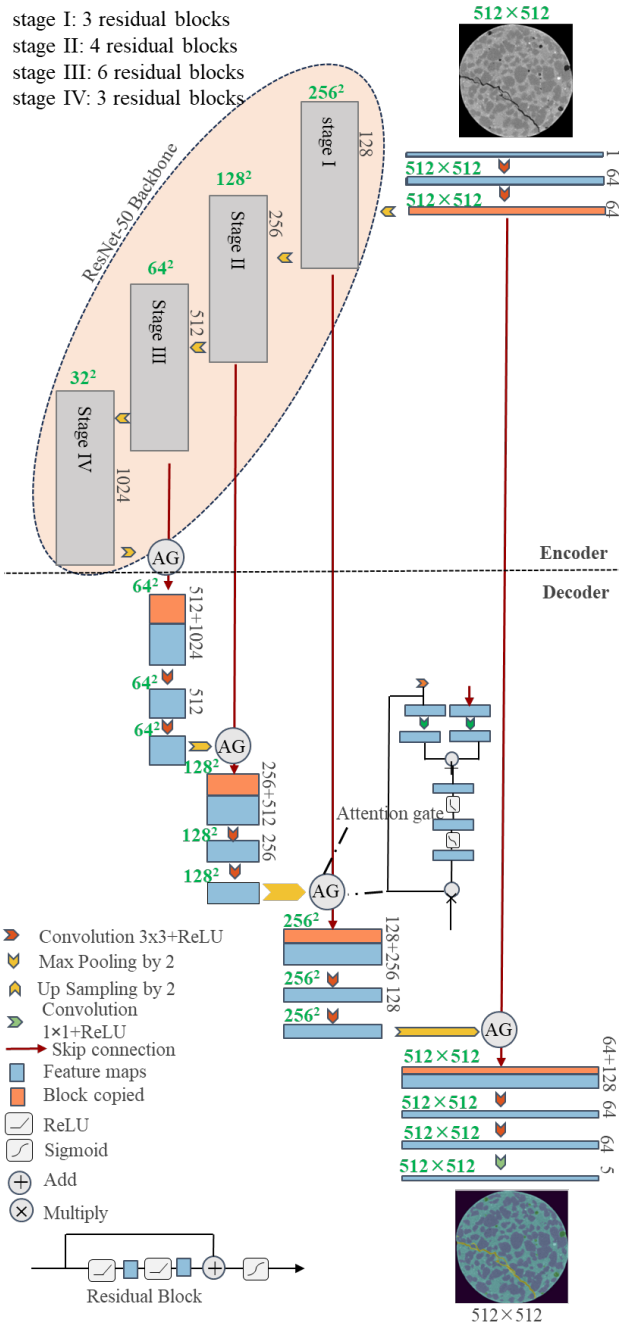

Figure 1: Architecture of U-net with ResNet50 and SCSE attention gate

2.2 Semantic segmentation model for XCT data analysis

This study trained a semantic segmentation model based on a 2D U-Net architecture with a ResNet50 encoder to segment XCT data by processing the XY slices. The model with a detailed architecture in Figure 1 utilizes pre-trained weights from ImageNet[18] for the encoder, which helps leverage the powerful feature extraction capabilities of ResNet50. Additionally, SCSE attention mechanisms[19] were incorporated in the decoder to enhance feature extraction by recalibrating the feature maps both spatially and channel-wise.

The model was configured with a single input channel, as the XCT data is grayscale, and five output classes corresponding to the segmentation targets: background, aggregate particles, cement matrix, pores, and cracks. The model was implemented using the Segmentation Models PyTorch library[20], which provides a high-level API for building and training segmentation models.

$$Loss = DiceLoss + CrossEntropyLoss$$
$$= (1 - \frac{2TP}{2TP + FP + FN}) + (-\sum_i y_i \cdot \log(p_i)) \quad (1)$$

True Positives (*TP*) are correctly identified as the target, while False Positives (*FP*) are mistakenly classified when they are not. False Negatives (*FN*) are pixels that are incorrectly predicted as non-target. The variable y_i is 1 if pixel *i* belongs to the target and 0 if it is part of the background. The variable p_i represents the predicted probability that pixel i is the target.

The training process employed a combined loss function of Dice and Cross-Entropy Loss in Eq(1). The Dice Loss helps to maximize the overlap between the predicted and ground truth segmentation masks, while the Cross-Entropy Loss penalizes the misclassification of pixels. The class weights were balanced using the logarithmic values of the class ratios to address the class imbalance issue. The calculated weights are: [0.0201, 0.0121, 0.0127, 0.2828, 0.6722]. This approach ensures that the loss function gives more importance to underrepresented classes, thereby improving the model's performance on these classes.

56 XY slices of the XCT data were selected with a copped size of 512 x 512. Data augmentation techniques, such as random flipping, affine transformations, and contrast adjustments, were applied to the training data to improve the model's generalization ability. The dataset was split into training and validation sets, with a 70-30 split, and the patches were used to train the model.

The model was trained using the AdamW[21] optimizer with a learning rate of 1×10^{-4} and a weight decay of 1×10^{-4}. The learning rate was decreased to 10% of its current value if the validation loss failed to improve for more than 10 consecutive epochs. The training process also employed mixed precision training using GradScaler to speed up the training and reduce memory usage.

An early stopping strategy was employed to prevent overfitting and reduce unnecessary computation. Training was terminated if the validation loss did not significantly improve for 15 consecutive evaluations. This method halted the training process when further progress was unlikely. The intersection over union (*IoU*), as defined in Eq.(2), was used to evaluate the segmentation accuracy of the model during the training phase.

$$IoU = TP/(TP + FP + FN) \quad (2)$$

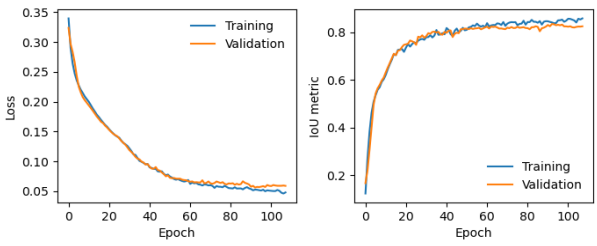

Figure 2: The model training: loss and IoU values over epochs.

The model was trained with a batch size of 4 using resources provided by the DTU HPC Computing Center (https://www.hpc.dtu.dk/), specifically 6 nodes with 2 x Tesla V100 16 GB GPUs (owned by DTU Compute & DTU Elektro) in the gpuv100 queue. As shown in

Figure 2, the model converged after 108 epochs, achieving an IoU of 83.51% and a loss of 5.63% on the validation set. Figure 3 shows selected predicted results on 5 images of the validation data, demonstrating the model's strong generalization capability.

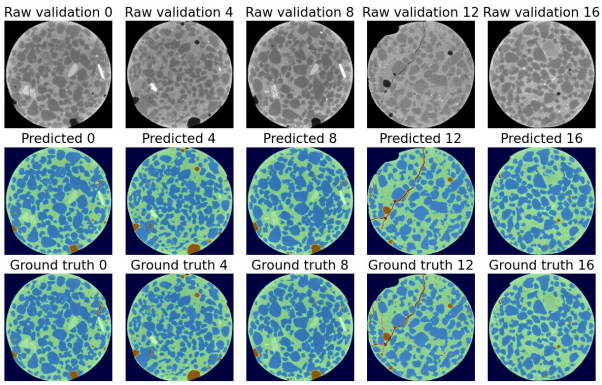

Figure 3: Comparison of raw images, labeled images, and predicted results on the validation dataset.

Table 1 presents the model's performance metrics on the validation dataset. Precision indicates that 89.54% of the pixels predicted as positive are positive, reflecting the model's ability to avoid false positives. Recall shows that 86.18% of the actual positive pixels are correctly identified, indicating the model's effectiveness in detecting true positives. Accuracy, at 96.33%, represents the overall correctness of the model's predictions across all classes. The F1 Score, the harmonic mean of Precision and Recall, balances the trade-off, providing a single score reflecting the model's effectiveness in identifying true positives and avoiding false positives. These metrics demonstrate the model's strong performance in accurately segmenting the validation data.

Table 1: Performance metrics of the model on the validation dataset

Metric	Precision	Recall	Accuracy	*F1*
Score	0.8954	0.8618	0.9633	0.8676

3. RESULTS

Five 3D XCT images were segmented using the trained model, including the reference image without load, images after monotonic loading to 600N, and images after 10, 50, and 200 cycles. Three orthogonal slices are shown, as illustrated in Figure 4.

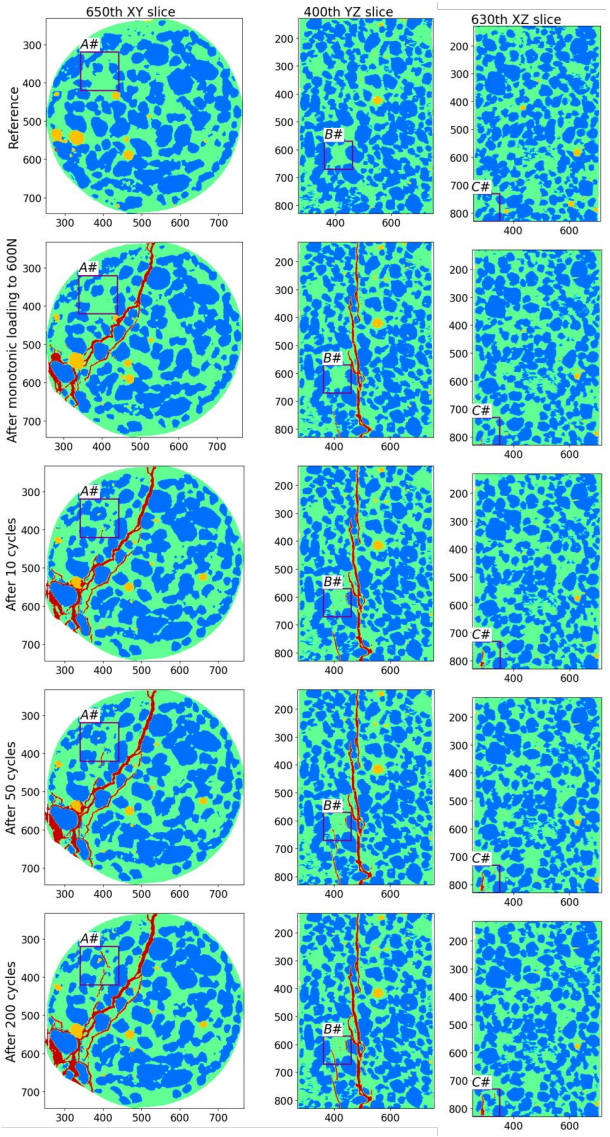

Figure 4: Three orthogonal slices of the segmentation results for the reference image without load, images after monotonic loading to 600N, and images after 10, 50, and 200 cycles, from top to bottom. The 650th XY, 400th YZ, and 630th XZ slices are selected. In the images, red represents cracks, yellow indicates pores, dark blue denotes aggregate, and green signifies the cement matrix. The axis scale is measured in pixels, and the loading is along the Z direction.

From Figure 4, it can be observed that a significant crack nearly spans the entire sample after monotonic loading to 600N. As cyclic loading continues, fine cracks initiate and grow in other areas, such as regions *A#*, *B#*, and *C#*. These regions were cropped and zoomed in to

identify this further, as shown in Figure 5.

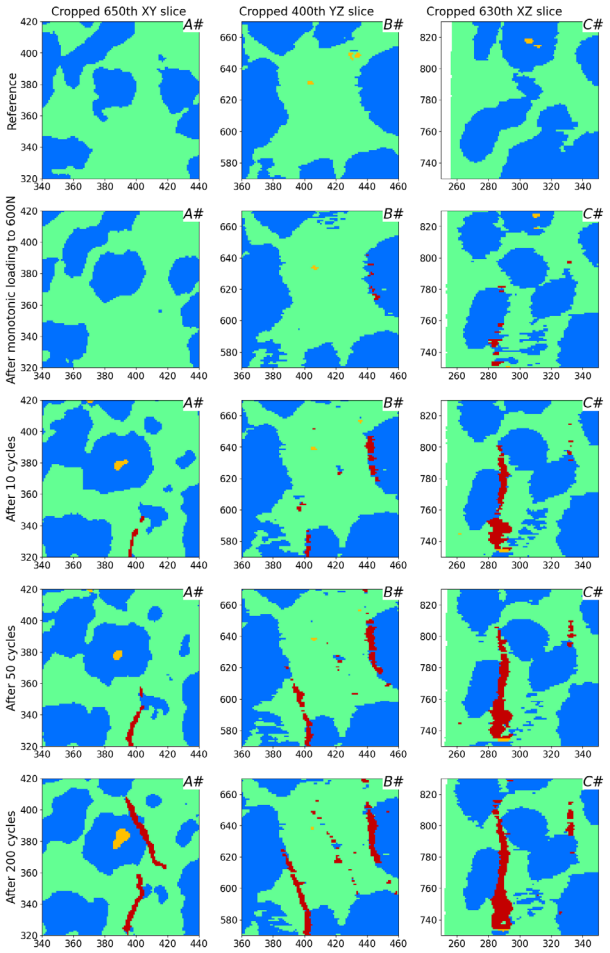

Figure 5: Cropped and zoomed-in views of regions A#, B#, and C# highlighting crack (red bands) initiation and growth after monotonic and cyclic loading. The axis scale is measured in pixels.

From Figure 5, two primary cracking behaviors during fatigue cycles are evident. Small cracks emerge during cyclic loading through two primary mechanisms. First, sudden crack formation occurs within the cement matrix in regions without pre-existing defects, as observed in A# after 10 loading cycles. Furthermore, the sudden appearance of cracks in the cement matrix suggests the presence of microcracks formed during earlier cycles that were below the resolution of XCT imaging. This observation is consistent with earlier findings [22] that a higher density of nanoscale cracks, with widths less than 500 nm, were present in the cement paste under cyclic loading. With continued cyclic loading, these microcracks grow rapidly and eventually become detectable. Second, cracks often initiate within ITZ, particularly in areas exhibiting microcracks or defects from prior monotonic loading, as highlighted by the red bands as cracks in B# and confirmed in C# after 10 cycles. The ITZ's inherent weaknesses and pre-existing damage make it a preferential site for crack initiation.

As loading progresses, existing cracks extend and connect to form a more extensive crack network, often propagating through the ITZ, as shown in C# from 10 to 200 cycles. This behavior aligns with established findings in the literature[23], which suggest that cracks propagate along paths of minimal energy by effectively linking pre-existing defects and weaknesses. Such propagation pathways are particularly evident in B# from 10 to 200 cycles, where cracks follow the ITZ or other energy-efficient routes. The observed patterns corroborate prior studies emphasizing the role of microstructural characteristics in guiding crack growth.

4 CONCLUSIONS

This study investigates the fatigue-induced cracking behaviors in cementitious materials using in-situ XCT imaging and a semantic segmentation model. The model, based on a U-Net architecture with a ResNet50 encoder and SCSE attention mechanisms, achieved high accuracy (96.33%) and IoU (83.51%), enabling precise identification of cracks, aggregates, cement matrix, and pores in XCT datasets. The analysis provides valuable insights into crack initiation and propagation mechanisms under cyclic loading.

Two primary mechanisms of cracking were identified during cyclic loading: (1) sudden crack formation within the cement matrix in regions where pre-existing defects are not visible at the micronmeter scale using XCT, but may exist at smaller scales and (2) crack initiation and propagation within the interfacial transition zone (ITZ), particularly in areas with pre-existing damage. The first mechanism, observed in region A# after 10 cycles, suggests that cracks in the cement matrix may have been initiated from microcracks formed during

earlier cycles, which were undetectable due to XCT resolution limitations. The second mechanism, observed in regions B# and C#, indicates that cracks preferentially initiated and propagated in the ITZ, which is more susceptible to damage due to pre-existing defects from monotonic loading. As cyclic loading progressed, these cracks grew and interconnected, forming an extensive crack network that primarily propagated through the ITZ and existing cracks, following paths of least resistance, i.e., minimizing the energy needed for fracture, as seen in regions B# and C# from 10 to 200 cycles.

These findings emphasize the ITZ's key role in fatigue damage, suggesting that improving its microstructure could reduce such damage. Additionally, using higher-resolution imaging techniques could enable the detection of nanoscale cracks at earlier stages, providing deeper insights into the initial damage mechanisms. This would contribute to the development of more robust predictive models for fatigue behavior and help guide the design of cement-based materials with improved resistance to cyclic stress and longer service life.

ACKNOWLEDGMENTS

The presented work is part of the FRONTIER project, funded by VILLUM FONDEN. This research is an ongoing effort to reveal the actual fatigue damage process in engineering materials, using Digital Volume Correlation as the primary tool. The authors would like to thank the 3D Imaging Centre (3DIM) for providing the relevant software for analysis.

REFERENCES

[1] B. Chen, L. Guo, W. Sun, Fatigue performance and multiscale mechanisms of concrete toughened by polymers and waste rubber, Advances in Materials Science and Engineering, 2014 (2014) 684207.

[2] N.H. Nguyen, H.H. Bui, J. Kodikara, S. Arooran, F. Darve, A discrete element modelling approach for fatigue damage growth in cemented materials, International Journal of Plasticity, 112 (2019) 68-88.

[3] K.M. Simon, J.C. Kishen, A multiscale approach for modeling fatigue crack growth in concrete, International Journal of Fatigue, 98 (2017) 1-13.

[4] H. Zhang, B. Šavija, S.C. Figueiredo, E. Schlangen, Experimentally validated multi-scale modelling scheme of deformation and fracture of cement paste, Cement and Concrete Research, 102 (2017) 175-186.

[5] S. Dutta, J.C. Kishen, Mesoscale analysis of fatigue damage through aggregate–mortar bond cracks in cementitious composites, Journal of Engineering Mechanics, 146 (2020) 04019126.

[6] G.M. Nordby, Fatigue of concrete-a review of research, Journal Proceedings, 1958, pp. 191-219.

[7] J.W. Murdock, A critical review of research on fatigue of plain concrete, University of Illinois. Engineering Experiment Station. Bulletin; no. 475, (1965).

[8] M. Lee, B. Barr, An overview of the fatigue behaviour of plain and fibre reinforced concrete, Cement and Concrete Composites, 26 (2004) 299-305.

[9] K. Kirane, Z.P. Bažant, Microplane damage model for fatigue of quasibrittle materials: Sub-critical crack growth, lifetime and residual strength, International Journal of Fatigue, 70 (2015) 93-105.

[10] P. Nowakowski, C. Bonifacio, M. Ray, P. Fischione, Advances in Beam-sensitive Sample Preparation and Observation, Microscopy and Microanalysis, 28 (2022) 2214-2215.

[11] M. Noorsuhada, An overview on fatigue damage assessment of reinforced concrete structures with the aid of acoustic emission technique, Construction and Building Materials, 112 (2016) 424-439.

[12] N. Oneschkow, T. Timmermann, S. Löhnert, Compressive fatigue behaviour of high-strength concrete and mortar: Experimental investigations and computational modelling, Materials, 15 (2022) 319.

[13] K. Keerthana, J.C. Kishen, An experimental and analytical study on fatigue damage in concrete under variable amplitude loading, International Journal of Fatigue, 111 (2018) 278-288.

[14] H. Zeng, W. Li, M. Jin, J. Zhang, Y. Ma, C. Lu, J. Liu, Deterioration of performances and structures of cement pastes under the action of thermal cycling fatigue, International Journal of Fatigue, 165 (2022) 107181.

[15] W. Ren, Z. Yang, R. Sharma, C. Zhang, P.J. Withers, Two-dimensional X-ray CT image based meso-scale fracture modelling of concrete, Engineering Fracture Mechanics, 133 (2015) 24-39.

[16] F. Aldakheel, A microscale model for concrete failure in poro-elasto-plastic media, Theoretical and Applied Fracture Mechanics, 107 (2020) 102517.

[17] C. Kuang, S. Ghosh, A. Michel, Enhanced detection of fine damage in composite materials using integrated X-ray computed tomography, digital volume correlation, and U-Net, Journal of Building Engineering, 98 (2024) 111440.

[18] J. Deng, W. Dong, R. Socher, L.J. Li, L. Kai, F.-F. Li, ImageNet: A large-scale hierarchical image database, 2009 IEEE Conference on Computer Vision and Pattern Recognition, 2009, pp. 248-255.

[19] Z. Zhong, Z.Q. Lin, R. Bidart, X. Hu, I.B. Daya, Z. Li, W.-S. Zheng, J. Li, A. Wong, Squeeze-and-attention networks for semantic segmentation, Proceedings of the IEEE/CVF conference on computer vision and pattern recognition, 2020, pp. 13065-13074.

[20] P. Iakubovskii, Segmentation Models Pytorch, GitHub, 2019.

[21] P.K. Diederik, Adam: A method for stochastic optimization, (No Title), (2014).

[22] Y. Gan, H. Zhang, Y. Zhang, Y. Xu, E. Schlangen, K. van Breugel, B. Šavija, Experimental study of flexural fatigue behaviour of cement paste at the microscale, International Journal of Fatigue, 151 (2021) 106378.

[23] V.P. Nguyen, M. Stroeven, L.J. Sluys, Multiscale failure modeling of concrete: Micromechanical modeling, discontinuous homogenization and parallel computations, Computer Methods in Applied Mechanics and Engineering, 201 (2012) 139-156.